














A diverse, overlooked population of Type Ia supernovae exhibiting mid-infrared signatures of delayed circumstellar interaction

GEOFFREY MO ¹, KISHALAY DE ^{1,*}, ELI WISTON ², NAYANA A.J. ², RAFFAELLA MARGUTTI ^{2,3}, DANIELLE FROSTIG ⁴, JESPER SOLLERMAN ⁵, YASHVI SHARMA ⁶, TAKASHI J. MORIYA ^{7,8,9}, KEVIN B. BURDGE ¹, JACOB JENCSON ¹⁰, VIRAJ R. KARAMBELKAR ⁶ AND NATHAN P. LOURIE ¹

¹MIT Kavli Institute for Astrophysics and Space Research, 70 Vassar St., Cambridge, MA 02139, USA

²Department of Astronomy, University of California, Berkeley, CA 94720-3411, USA

³Department of Physics, University of California, 366 Physics North MC 7300, Berkeley, CA 94720, USA

⁴Center for Astrophysics | Harvard & Smithsonian, 60 Garden Street, Cambridge, MA 02138, USA

⁵The Oskar Klein Centre, Department of Astronomy, Stockholm University, AlbaNova, SE-10691 Stockholm, Sweden

⁶Division of Physics, Mathematics and Astronomy, California Institute of Technology, Pasadena, CA 91125, USA

⁷National Astronomical Observatory of Japan, National Institutes of Natural Sciences, 2-21-1 Osawa, Mitaka, Tokyo 181-8588, Japan

⁸Graduate Institute for Advanced Studies, SOKENDAI, 2-21-1 Osawa, Mitaka, Tokyo 181-8588, Japan

⁹School of Physics and Astronomy, Monash University, Clayton, VIC 3800, Australia

¹⁰IPAC, Mail Code 100-22, Caltech, 1200 E. California Blvd., Pasadena, CA 91125, USA

(Dated: January 31, 2025)

ABSTRACT

Type Ia supernovae arise from the thermonuclear explosions of white dwarfs in multiple star systems. A rare sub-class of SNe Ia exhibit signatures of interaction with circumstellar material (CSM), allowing for direct constraints on companion material. While most known events show evidence for dense nearby CSM identified via peak-light spectroscopy (as SNe Ia-CSM), targeted late-time searches have revealed a handful of cases exhibiting delayed CSM interaction with detached shells. Here, we present the first all-sky search for late CSM interaction in SNe Ia using a new image-subtraction pipeline for mid-infrared data from the *NEOWISE* space telescope. Analyzing a sample of ≈ 8500 SNe Ia, we report evidence for late-time mid-infrared brightening in five previously overlooked events spanning sub-types SNe Iax, SNe Ia-91T and super-Chandra SNe Ia. Our systematic search doubles the known sample, and suggests that $\gtrsim 0.05\%$ of SNe Ia exhibit mid-infrared signatures of delayed CSM interaction. The mid-infrared light curves ubiquitously indicate the presence of multiple (or extended) detached CSM shells located at $\gtrsim 10^{16} - 10^{17}$ cm, containing $10^{-6} - 10^{-4} M_{\odot}$ of dust, with some sources showing evidence for new dust formation, possibly within the cold, dense shell of the ejecta. We do not detect interaction signatures in spectroscopic and radio follow-up; however, the limits are largely consistent with previously confirmed events given the sensitivity and observation phase. Our results highlight that CSM interaction is more prevalent than previously estimated from optical and ultraviolet searches, and that mid-infrared synoptic surveys provide a unique window into this phenomenon.

Keywords: Type Ia supernovae (1728), Supernovae (1668), Infrared excess (788), Common envelope binary stars (2156), Interacting binary stars (801)

1. INTRODUCTION

It is well established that Type Ia supernovae (SNe Ia) arise from the thermonuclear explosions of white dwarfs (WDs), triggered by interaction with a companion star (Maoz et al. 2014). Not only do SNe Ia serve as standardizable candles (Branch & Tammann 1992; Phillips 1993; Kasen & Woosley 2007; Dhawan et al. 2018; Avelino et al. 2019), they probe a common end-point in binary stellar

Corresponding author: Geoffrey Mo
gmo@mit.edu

* MIT Kavli Institute Fellow

evolution (Wang & Han 2012; Postnov & Yungelson 2014; Ruiter 2020; Liu et al. 2023), reveal the fates of mHz gravitational wave sources (Toonen et al. 2012; Rebassa-Mansergas et al. 2019; Karnesis et al. 2021; Korol et al. 2024), and provide insights into the universal chemical and dust budget (Kobayashi & Nomoto 2009; Nozawa et al. 2011; Lach et al. 2020; Wang et al. 2024). However, the nature of the WD (mass; composition) and the companion (degenerate or not; accretion via mergers or mass transfer), as well as the explosion mechanism (detonation or deflagration) remain unresolved, with clear evidence for multiple channels (Pakmor et al. 2013; Ashall et al. 2016; Polin et al. 2019; Bulla et al. 2020; Hakobyan et al. 2020).

Supporting the diverse nature of progenitors, a rare sub-class of SNe Ia—known as SNe Ia-CSM ($\lesssim 0.2\%$ of SNe Ia; Silverman et al. 2013a; Sharma et al. 2023)—exhibit strong interaction of the expanding ejecta¹ with dense nearby circumstellar material (CSM). These events are typically identified via strong narrow emission lines (commonly H α) in spectroscopy acquired at or near peak light (Sharma et al. 2023), similar to Type II_n supernovae (Smith 2017). This H-rich material has been ubiquitously attributed to mass supplied by a non-degenerate companion, allowing for direct constraints on its composition and configuration. The proximity ($\lesssim 10^{15}$ cm) and large mass ($\gtrsim 0.1 M_{\odot}$) of the CSM have been explained via binary progenitors such as a WD merging with the core of an asymptotic giant branch (AGB) star inside (or shortly after the ejection) of the common envelope (i.e. the core-degenerate scenario; Tutukov et al. 1992; Livio & Riess 2003; Kashi & Soker 2011; Ablimit 2021) or even as a result of dynamical mass transfer from a main sequence star (Han & Podsiadlowski 2006). Since systematic searches (Silverman et al. 2013a; Sharma et al. 2023) have relied on peak-light spectroscopy or peculiar undulations in early-time light curves to identify candidates for SNe Ia-CSM, these are biased against SNe Ia with distant CSM shells where signatures of interaction would only be detectable at later phases (Sharma et al. 2023; Phillips et al. 2024).

Dilday et al. (2012) presented the first example of a SN Ia (of the 1991T subclass; see Blondin et al. 2012 and Taubenberger 2017 for a review of SN Ia sub-types) that transitioned to a Ia-CSM at late phases (> 40 d after

peak) due to the delayed CSM interaction in PTF11kx.² The multiple, detached CSM shells detected in this object were suggested to arise from a symbiotic nova progenitor (Han & Podsiadlowski 2004), although Soker et al. (2013) have argued for a core-degenerate scenario where the envelope was ejected shortly before the explosion. Using a *Hubble Space Telescope* (HST) ultraviolet photometric survey of 72 SNe, Graham et al. (2019) reported evidence for late CSM interaction in SN 2015cp, which was initially classified as a SN Ia-91T-like object. A search for similar emission in the GALEX archive yielded no additional detection (Dubay et al. 2022). Late-time spectroscopic signatures of interaction (via H α emission) have also been reported in SN 2016jae (Elias-Rosa et al. 2021), SN 2018cqj (Prieto et al. 2020), and SN 2018fhw (Kollmeier et al. 2019; Valley et al. 2019), while Kool et al. (2023) recently reported the first case of a SN Ia interacting with He-rich CSM. While systematic efforts have been previously made to identify potential candidates for late interaction with optical photometry alone (Terwel et al. 2024), developing a complete census either by continued spectroscopic monitoring or UV observations is challenging on large scales due to cost.

The mid-infrared (MIR) bands provide an independent and powerful approach to probing CSM interaction and associated dust formation (Szalai et al. 2019). Instead of directly detecting the high-energy X-ray or UV radiation produced by the shock interaction with the CSM, MIR observations detect emission from warm dust, which can either be pre-existing around the progenitor or be produced in the interaction region after explosion (Fox et al. 2011; Szalai & Vinkó 2013). When SN ejecta interact with surrounding CSM, dust can be heated by shock radiation, producing luminous late-time MIR emission (Fox et al. 2015). MIR brightening episodes therefore provide a unique tool to detect CSM interaction at late phases, but systematic searches remain limited without synoptic MIR capabilities. Myers et al. (2024) have recently reported a systematic search for late MIR emission in core-collapse supernovae from *NEOWISE* data (Wright et al. 2010; Mainzer et al. 2014), demonstrating the potential of all-sky, slow cadence surveys in revealing the demographics of CSM interaction.

In this Letter, we report the identification of an overlooked population of recent SNe Ia exhibiting delayed CSM interaction. Capitalizing on the rapid growth of large SN samples from all-sky time-domain optical surveys such as ZTF (Bellm et al. 2018), ATLAS (Tonry

¹ We note that interaction with very nearby CSM can also be detected as early-time excesses in optical light curves or high velocity features (e.g., Noebauer et al. 2016; Mulligan & Wheeler 2017; Moriya et al. 2023); however, we do not discuss them here since existing observations do not conclusively rule out other possibilities (e.g. Childress et al. 2014; Deckers et al. 2022).

² Harris et al. (2018) names these SNe Ia;_n to indicate the late-time emergence of narrow (“n”) emission lines.

et al. 2018), ASAS-SN (Kochanek et al. 2017), Pan-STARRS (Chambers et al. 2016), and Gaia (Hodgkin et al. 2021), we present a complete search of *NEOWISE* data for MIR excesses using a new image subtraction pipeline. We begin by characterizing the MIR behavior of known SNe Ia with delayed CSM interaction, and a search for new similar objects in Section 2. We use the MIR emission together with follow-up observations to constrain the amount and configuration of the CSM shells in Section 3. We conclude by discussing the implications for this overlooked population in Section 4. Throughout, we assume Planck18 cosmology (Planck Collaboration et al. 2020).

2. OBSERVATIONS

2.1. MIR behavior of known SNe Ia with late CSM interaction

Using data from the infrared *Spitzer Space Telescope* (Werner et al. 2004), Fox & Filippenko (2013) reported luminous, brightening late-time MIR emission in SNe Ia-CSM 2002ic and 2005gj, suggesting renewed shock interaction with CSM shells. Subsequently, Szalai et al. (2019), Szalai et al. (2021) and Sharma et al. (2023) also confirmed consistently bright late-time MIR emission in larger samples of SNe Ia-CSM based on *Spitzer* and *NEOWISE* observations, largely consistent with pre-existing dust heated by ongoing CSM interaction. A similar, luminous MIR excess was also reported in the case of the nearby SN Iax 2014dt (Fox et al. 2016; Jenson et al. 2019), although its origin has been debated (as arising from circumstellar dust or possibly a bound remnant; Foley et al. 2016). Using a comprehensive spectral sequence and *NEOWISE* observations, Wang et al. (2024) provided evidence for multiple dust shells as well as new late-time dust formation in the SN Ia-CSM 2018evt. To understand if MIR searches can be fruitful to look for delayed CSM interaction in SNe Ia, we first investigate previously known events in *NEOWISE* data. The *NEOWISE* survey’s all-sky coverage, MIR photometric bands ($W1 \approx 3.4 \mu\text{m}$, $W2 \approx 4.6 \mu\text{m}$), long baseline (≈ 13 yr), regular cadence (≈ 6 month), and sensitivity (≈ 20 AB mag) are ideal attributes for such a search. When combined with a new difference photometry pipeline (De et al., in prep) with unWISE coadded images (Lang 2014; Meisner et al. 2018) and a ZOGY-based subtraction algorithm (Zackay et al. 2016; De et al. 2020) adept at recovering faint transients on bright hosts, this MIR dataset has already proven to be powerful for core-collapse SNe (Myers et al. 2024).

NEOWISE observations of PTF11kx begin ≈ 3.5 yrs after peak light, exhibiting luminous emission detected for two more years (also previously reported with *Spitzer*

data in Graham et al. 2017). Similarly, the *NEOWISE* analysis of SN 2015cp reveals a long-lasting MIR light curve³. We show a comparison of these light curves with SNe Ia-CSM in Figure 1, and their individual light curves in Figure A1. Kool et al. (2023) reported luminous MIR emission from SN 2020eyj that exhibited delayed interaction with a He-rich CSM shell. In contrast, *NEOWISE* light curves of the sub-luminous SNe Ia which show late-time H α emission (SNe 2016jae, 2018cqj, and 2018fhw), as well as the candidates identified from late-time optical photometry (Terwel et al. 2024) (SNe 2018grt, 2019ldf, and 2020tfc) do not show luminous MIR emission comparable to the other events. We discuss possible reasons in Section 3.3. As shown in Figure 1, many SNe Ia-CSM and SNe Ia with delayed CSM interaction show luminous late-time MIR emission, distinct from normal SNe Ia, making MIR searches a promising avenue for identifying this phenomenon.

2.2. Systematic search in *NEOWISE* for missed events

We produced *NEOWISE* MIR difference imaging light curves for ≈ 8500 Type Ia SNe from 2011 to 2022⁴ reported to the IAU Transient Name Server⁵. These light curves were visually inspected to search for late-time MIR emission associated with the SN. We filter the light curves by i) rejecting candidates with detections prior to the optical onset of the SN (to remove contamination from active galactic nuclei activity) or obvious subtraction artifacts; and ii) requiring at least two epochs of *NEOWISE* detections (≈ 1 yr) and rising emission in at least one band, to conclusively rule out excess MIR emission arising purely from new dust formation or a SN light echo without added power from shock-interaction, and to eliminate detections deemed to only be associated with photospheric emission from the optical SN. Most of the identified candidates were known SNe Ia-CSM; we do not discuss them here as their light curves have been presented in Sharma et al. (2023). Table A1 summarizes the cuts at each filtering stage. Notably, these selection criteria resulted in the identification of five candidates which exhibit luminous late-time MIR emission despite not being previously associated with CSM interaction.⁶

³ Thévenot et al. (2021a) previously also reported the *NEOWISE* detection of SN 2015cp.

⁴ The 2022 cutoff is governed by the availability of unWISE data products.

⁵ <https://www.wis-tns.org>

⁶ SN 2020mvp (Tonry et al. 2020) also emerged as a candidate, but further astrometric inspection of the *NEOWISE* imaging revealed that the MIR emission was likely from temporally coincident nuclear activity.

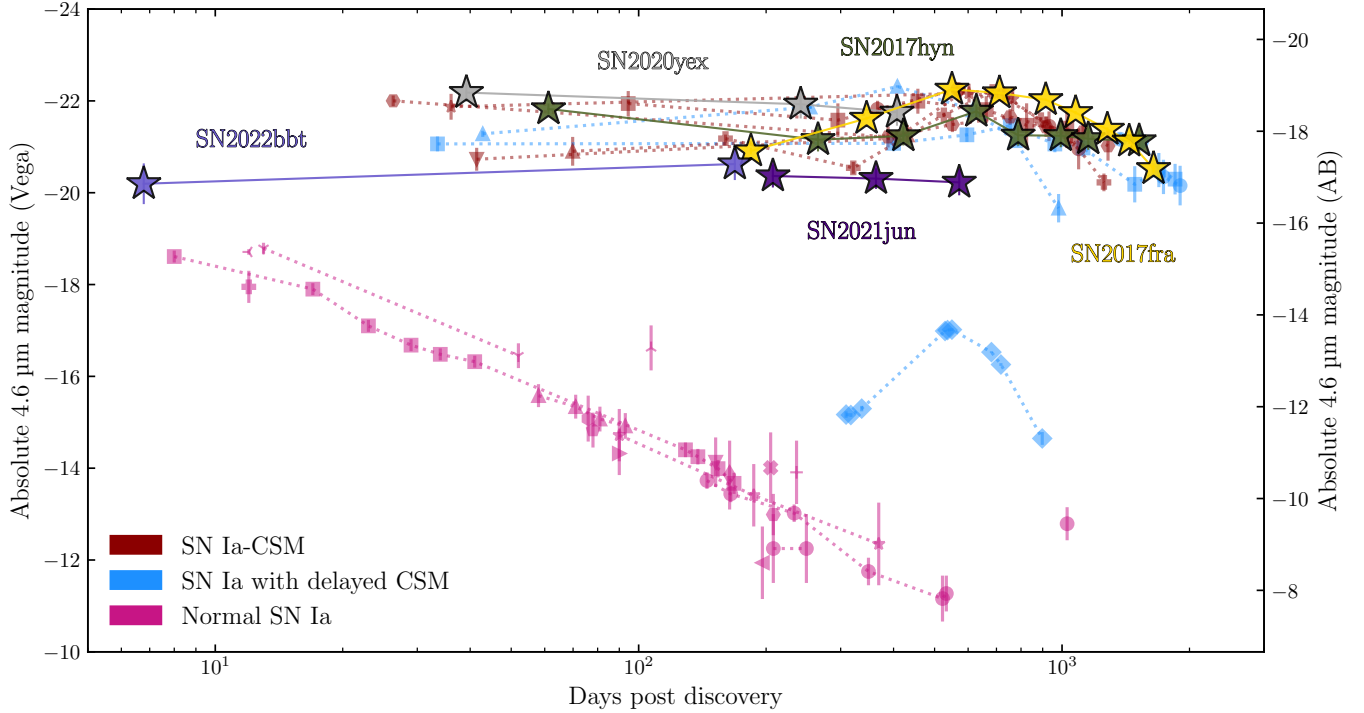


Figure 1. The phase space of mid-infrared light curves for SNe Ia. We show *NEOWISE* *W2* light curves for the SNe Ia showing delayed CSM interaction from our sample in the colored stars. For comparison, we also plot previously published SNe Ia with delayed CSM interaction, including PTF11kx, SN 2015cp, and SN 2020eyj (blue circles, squares, and triangles respectively). Plotted in the blue diamonds is the *Spitzer* IRAC Ch2 light curve of SN 2014dt, a SN Iax which exhibits an analogous rise and fall to the interacting SNe Ia, but at a much lower luminosity (Fox et al. 2016; Jencson et al. 2019). The SNe Ia-CSM, for which we show selected *W2* light curves in dark red (these include SNe 2016iks, 2017eby, 2017hzw, 2018crl, 2018evt, 2018gkx, 2019agi, 2020aekp), display similar behavior to most of the SNe Ia with delayed CSM interaction. Finally, we show *Spitzer* Ch2 light curves of normal SNe Ia from Szalai et al. (2019) in magenta.

The candidates span multiple Type Ia subclasses: SN 2017fra (originally classified as a SN Ia-91T), SN 2017hyn (Ia-91T), SN 2020yex (Ia-91T), SN 2021jun (Iax), and SN 2022bbt (super-Chandra Ia)⁷. We summarize these SNe in Table 1, further describe each in Appendix A, and show reference, science, and difference image cutouts in Figure A2. While half of our sample are SNe Ia-91T-like, strengthening the established connection between SNe Ia-CSM and SNe Ia-91T (Leloudas et al. 2015), we report the first detection of late-time MIR brightenings in a super-Chandra SN Ia,⁸ and the second detection of an MIR excess in a SN Iax. We show a comparison of their MIR light curves in Figure 1, and the

individual optical and MIR light curves of these events in Figure 2. Compared to normal SNe Ia, our newly identified events have significant MIR excesses reaching luminosities of $W2 \approx -22$ Vega mag, lasting hundreds to thousands of days. Of note is the MIR light curve of the SN Iax 2014dt, which shows similar behavior to but is much less luminous than the rest of the interacting SNe Ia; its late MIR rise has been suggested to arise from newly formed dust, but could also be attributable to pre-existing CSM or a bound remnant (Fox et al. 2016; Foley et al. 2016; Jencson et al. 2019).

2.3. Multi-wavelength follow-up observations

We performed optical spectroscopic follow-up of two of the youngest events⁹: SN 2020yex ($z = 0.087$) and SN 2022bbt ($z = 0.049$). We also performed radio follow-up of SN 2022bbt. Optical spectroscopic observations were carried out using a Fast Turnaround Program on the Gemini North and Gemini South telescopes (Program IDs

⁷ Thévenot et al. (2021a) and Thévenot et al. (2021b) have previously noted MIR detections for SN 2017hyn, SN 2017fra, and SN 2020yex; Jiang et al. (2021) previously analyzed *NEOWISE* observations of SN 2017fra in their search for MIR flares in nearby galaxies.

⁸ The super-Chandra SNe Ia SN 2012dn (Nagao et al. 2017) and SN 2022pul (Siebert et al. 2024) have previously reported MIR excesses, but the lack of a detected MIR brightening are consistent with SN light echoes or new dust formation in cooling ejecta.

⁹ We did not follow up SN 2021jun due to its proximity to its host nucleus, which would make faint object spectroscopy challenging.

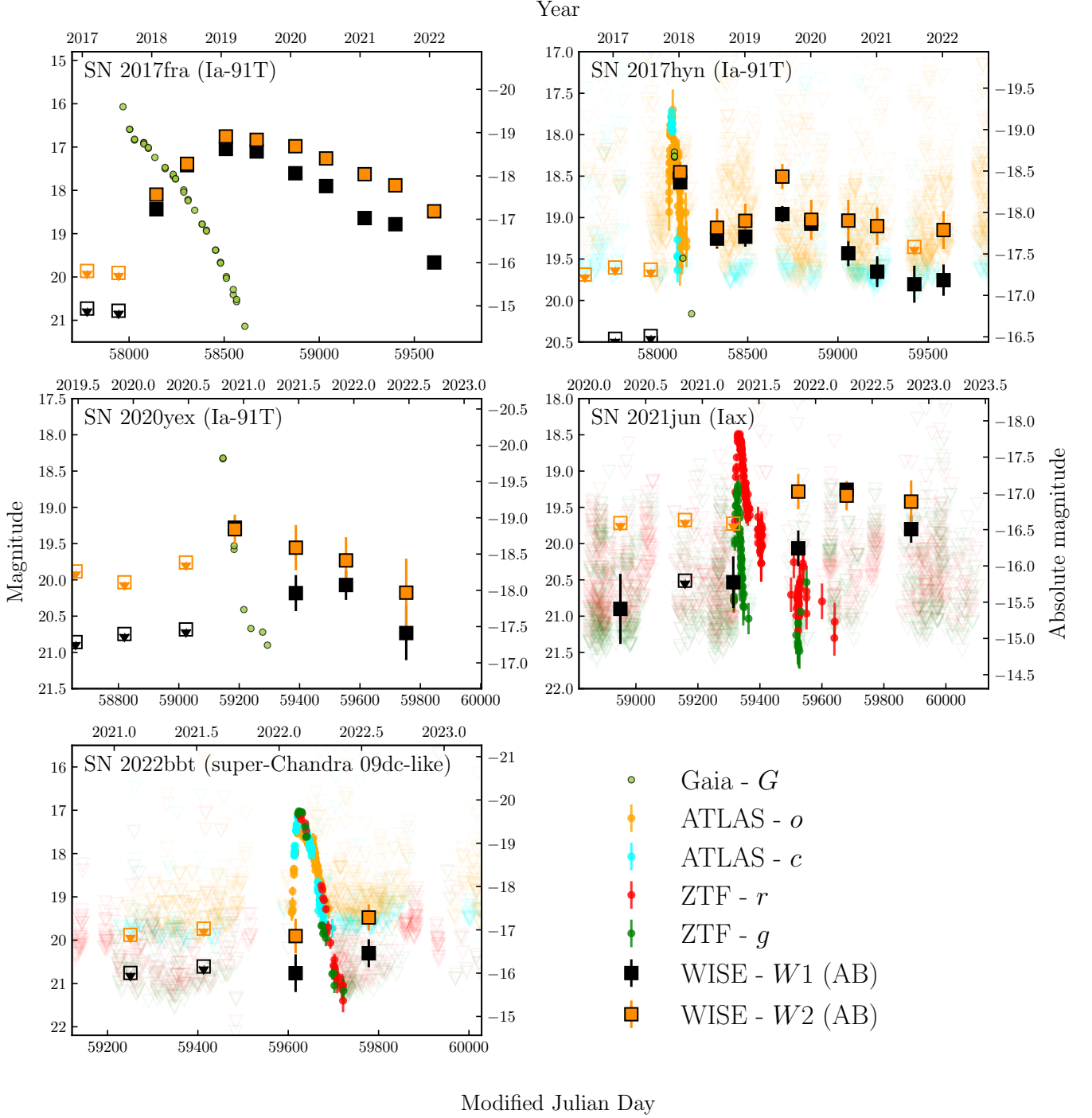


Figure 2. Optical and mid-infrared light curves of our sample of Type Ia SNe showing evidence for delayed CSM interaction. We show *NEOWISE* MIR light curves alongside Gaia, ATLAS, and ZTF photometry of the SNe in our sample. Upper limits are displayed as downward pointing empty markers. In parentheses next to each SN’s label is its peak-light classification.

GN-2024B-FT-102/GS-2024B-FT-102; PI: Mo), while radio observations were carried out using the Karl G. Jansky Very Large Array (VLA) under the Director’s Discretionary Program (VLA/24A-498; PI: Nayana AJ). In addition, we obtained NIR spectroscopy of SN 2020yex and NIR imaging of SN 2017fra using the Magellan Baade

telescope, and NIR imaging of SN 2021jun with *WIN-TER* (Lourie et al. 2020; Frost et al. 2024). Further details about the observations and data reduction can be found in Appendix B. We do not detect photometric or spectroscopic signatures of CSM interaction in any of our optical/NIR observations while the VLA observations

Table 1. Summary of our SNe Ia showing MIR signs of delayed CSM interaction. The integrated energy is calculated by integrating the detected W2 fluxes.

Name	Type	Host morphology	Redshift	Distance [Mpc]	Peak W2 AB magnitude	Integrated W2 energy [erg]
SN 2017fra	Ia-91T	Interacting spiral	0.03	136	16.8	7.9×10^{49}
SN 2017hyn	Ia-91T	Edge-on disk	0.053	244	18.5	5.4×10^{49}
SN 2020yex	Ia-91T	Blue spheroidal	0.087	425	19.3	2.3×10^{49}
SN 2021jun	Iax	Blue spheroidal	0.040	183	19.3	5.2×10^{48}
SN 2022bbt	Ia-SC	Face-on spiral	0.049	225	19.5	2.8×10^{49}

also did not detect a radio counterpart. We discuss the implications of these non-detections in Section 3.3.

3. ORIGIN OF THE MIR EMISSION

We have identified a sample of five SNe Ia showing clear evidence for late-time MIR brightenings. While fading excess late-time MIR emission can be caused by a light echo from the SN or dust formation in the cooling ejecta, rebrightening in the MIR light curve indicates the presence of an internal energy source (i.e., high-energy radiation in the form of UV or X-ray photons) that is heating pre-existing or newly-formed dust (Fox et al. 2010, 2011). The lack of observed UV or X-ray emission from these events is unsurprising given the non-existence of all sky UV/X-ray surveys and the expected luminosity of the shock interaction radiation. For the observed peak W2 MIR luminosity of $\sim 10^{42} \text{ erg s}^{-1}$, the equivalent peak X-ray flux for sources at $\gtrsim 200 \text{ Mpc}$ would be $\sim 10^{-13} \text{ erg cm}^{-2} \text{ s}^{-1}$, which is far below the detection threshold of existing X-ray all-sky surveys ($\sim 10^{-11} \text{ erg cm}^{-2} \text{ s}^{-1}$ for MAXI/GSC, Hiroi et al. 2013; $\sim 10^{-10} \text{ erg cm}^{-2} \text{ s}^{-1}$ for Swift/BAT, Krimm et al. 2013), and may be detectable only with pointed X-ray follow-up (which does not exist for these sources). Furthermore, targeted X-ray observations of other SNe Ia have had limited success due to the rarity (one known event in SN 2012ca; Bochenek et al. 2018) and low luminosity ($L_X \lesssim 10^{37} \text{ erg s}^{-1}$ for normal SNe Ia from Margutti et al. 2014; $L_X \lesssim 10^{40} \text{ erg s}^{-1}$ for SNe Ia with delayed CSM interaction from Dwarkadas 2023, 2024) of X-ray emission associated with SNe Ia.

Given that known SNe Ia exhibiting delayed CSM interaction (see Figure 1) also show late-time MIR brightenings, these observations strongly suggest that the brightenings are powered by the onset of CSM interaction, where the shock of the high-velocity SN ejecta impacting existing CSM creates high-energy radiation that is absorbed and reemitted by dust. The integrated MIR energies shown in Table 1 span approximately 1-10% of the $\sim 10^{51} \text{ erg}$ in kinetic energy released in a SN Ia due to the efficient conversion of kinetic energy to radiative

energy during the shock; these shocks can convert up to $\sim 50\%$ of the total kinetic energy into radiative energy for interacting core-collapse SNe with similar CSM interaction (Smith 2017). The lack of spectroscopic signatures or optical light curve abnormalities at peak-light indicate that this sample represents an overlooked population of SNe Ia undergoing delayed CSM interaction. In this section, we use the *NEOWISE* multi-band photometry to constrain the mass, temperature, and location of the emitting dust to infer the CSM properties. We assume a spherical configuration for the dust for simplicity, though our limited observations cannot rule out complex geometries which may affect the light curve or inferred parameters only up to order unity corrections. In addition to the five SNe, we also fit the *NEOWISE* data from SN 2015cp, for comparison to a well-studied event.

3.1. Dust modeling

We first fit the *NEOWISE* photometry to a pure blackbody, described by

$$F_\nu = \frac{r_{\text{bb}}^2}{D^2} \pi B_\nu(T_{\text{bb}}), \quad (1)$$

where F_ν is the observed spectral flux density, r_{bb} is the blackbody radius, D is the distance to the source, and T_{bb} is the blackbody temperature. Given that the dust is not expected to emit as a pure blackbody source and may be optically thin, the derived r_{bb} is a lower limit to the true radius of the dust shell. Assuming the dust to be optically thin, the dust mass and temperature are described by

$$M_d = \frac{4a\rho D^2 F_\nu}{3Q_\nu \pi B_\nu(T_d)}, \quad (2)$$

where M_d is the dust mass, a is the dust size, ρ is the mass density of the dust, Q_ν is a dimensionless quantity describing the dust emissivity at frequency ν for dust size a , B_ν is the Planck function, and T_d is the dust temperature (Hildebrand et al. 1977). We assume a dust grain size of $0.1 \mu\text{m}$, a composition of carbonaceous grains, a dust mass density of $\rho = 2.2 \text{ g cm}^{-3}$ (Draine &

Li 2007), and we use the emissivity function for graphite dust from [Draine & Li \(2001\)](#). Fits with different dust composition (silicate vs graphite), grain size ($0.01\ \mu\text{m}$ vs $0.1\ \mu\text{m}$), and dust mass density ($1\ \text{g cm}^{-3}$ vs $2.2\ \text{g cm}^{-3}$ vs $5\ \text{g cm}^{-3}$) resulted in similar results, with dust masses within factors of a few and consistent dust temperatures. Since this fit assumes optically thin dust, and we lack observations at longer wavelengths which may help better constrain the dust, these are lower limits on dust masses. The evolution of our fit parameters is shown in Figure 3.

3.2. Constraints on CSM configuration

The top panel of Figure 3 shows the blackbody radius evolution compared to the ejecta radius of the SN. For all events, the blackbody radius is outside the ejecta radius at early times ($< 300\ \text{d}$), indicating that the emission at those times is powered by pre-existing dust. With an early SN luminosity of $\sim 10^{42} - 10^{43}\ \text{erg s}^{-1}$, the vaporization radius for graphite-rich $0.1\ \mu\text{m}$ grains is a few $\times 10^{16}\ \text{cm}$ ([Fox et al. 2010](#)), consistent with the survival of dust at the derived scales. Figure 3 also shows that the radii of the largest dust shells are comparable to the light travel time for the epoch of observation, suggesting that pre-existing dust is likely immediately re-radiating the optical SN light as a dust echo. A dust shell with a radius of a few $\times 10^{16}\ \text{cm}$ dictates that an observed dust echo cannot last longer than $\sim 100\ \text{d}$ given the typical duration of a SNIa and the light travel time across the shell. In addition, the available peak-light spectra do not show evidence of CSM interaction, indicating that the early-onset MIR emission is likely powered by the SN light itself.

Throughout our sample, we observe continued MIR emission beyond $\gtrsim 100\ \text{d}$, with a subsequent rise in the MIR light curve at $\approx 1 - 2\ \text{yrs}$ after explosion that is accompanied by a rise in the dust temperature. This indicates that pre-existing dust is being re-heated by the SN ejecta interacting with existing CSM at $\sim 10^{16}\ \text{cm}$, assuming a typical ejecta velocity of $10^4\ \text{km s}^{-1}$. Given that the pre-existing dust is typically at a larger radius, the observations suggest the presence of multiple CSM shells, as inferred for both SNeIa-CSM ([Fox & Filippenko 2013; Wang et al. 2024](#)) and previous SNeIa displaying delayed CSM interaction ([Dilday et al. 2012](#)). However, we cannot rule out the possibility that the SNe are surrounded by single, detached thick shells (with outer-to-inner radius ratio $\gtrsim \text{few}$). At early times, we additionally constrain the pre-existing dust mass to be $\sim 10^{-6} - 10^{-4}\ M_{\odot}$ in all the events.

The subsequent emission at later times ($\gtrsim 2\ \text{yr}$), in events for which we have well-sampled late-time MIR light curves, have blackbody radii within the ejecta radius

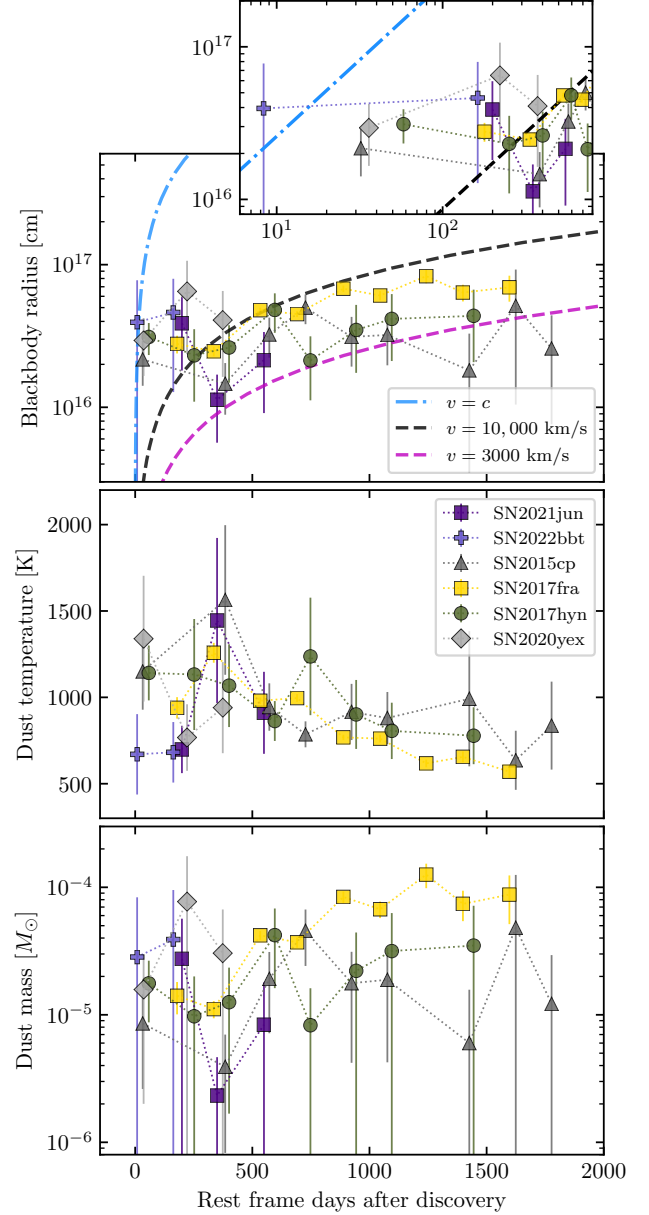


Figure 3. The evolution of dust properties, derived from fitting the *NEOWISE* *W1* and *W2* bands for events in our sample, as well as for SN 2015cp. *Top*: Lower limits on the blackbody radii compared to the speed-of-light (blue line), $10^4\ \text{km s}^{-1}$ ejecta (black line; relevant for typical SNeIa), and $3000\ \text{km s}^{-1}$ ejecta (magenta line; relevant for SNeIax). Note that the dust radii at early phases are far outside the ejecta, as shown in the inset. *Middle*: Dust temperatures assuming $0.1\ \mu\text{m}$ carbonaceous grains. There is a rise in the dust temperature at $\approx 1\ \text{yr}$ after explosion, indicating the reheating of pre-existing dust by radiation produced by CSM interaction. *Bottom*: The evolution of the dust mass shows an increase at later phases, consistent with the formation of new dust.

together with a slow increase that traces the ejecta radius evolution (SN 2015cp, SN 2017fra, and SN 2017hyn). When combined with the potentially increased dust mass, this suggests the formation of new dust, possibly within the cold, dense shell of the ejecta as it interacts with existing CSM, consistent with the formation of new dust reported for SN 2018evt (Wang et al. 2024), though the lack of spectral information prevents the drawing of firm conclusions.

3.3. Limits from spectroscopic and radio follow-up

We obtained follow-up spectroscopy of SN 2020yex and SN 2022bbt (described in Appendix B) with the goal of identifying broad or intermediate H or He lines typically seen in CSM-interacting SNe (Smith 2017; Graham et al. 2017, 2019). The left panel of Figure 4 shows the spectra extracted at the expected position of the SN. While we detect narrow emission lines from the host galaxy for SN 2020yex, we do not detect any broad or intermediate emission lines from either source, as seen in late-time spectra of PTF11kx and SN 2015cp. We derive 5σ upper limits on the $H\alpha$ luminosity of $L_{H\alpha,+1345d} < 7.5 \times 10^{39} \text{ erg s}^{-1}$ for SN 2020yex and $L_{H\alpha,+877d} < 1.9 \times 10^{38} \text{ erg s}^{-1}$ for SN 2022bbt (see Appendix B). To interpret these limits, we compare them to the evolution of the $H\alpha$ luminosity for PTF11kx and SN 2015cp, as well as with a SN IIn, known SNe Ia-CSM and other low-luminosity SNe Ia which show delayed CSM interaction via $H\alpha$ emission.

The right panel of Figure 4 shows that while the limits on SN 2022bbt are consistent with the fast $H\alpha$ decline of SN 2015cp (Graham et al. 2019), the non-detection rules out long-lived $H\alpha$ emission such as that seen in PTF11kx (Silverman et al. 2013b; Graham et al. 2017) and in SNe IIn (Tartaglia et al. 2020). Our non-detection of SN 2020yex rules out SN IIn-like long-lived $H\alpha$ emission. We additionally show the luminous MIR emission for these SNe in Figure 4. In contrast to $H\alpha$ emission which fades on 1 – 2 yr timescales for most interacting SNe Ia, the MIR emission is much longer-lived, lasting thousands of days. Compared to SNe Ia-CSM and SNe Ia showing delayed CSM interaction in the MIR, the population of events of subluminal SNe Ia with late-time $H\alpha$ emission (SN 2016jae, SN 2018cjj, and SN 2017fhw) exhibit $H\alpha$ luminosities which are $\sim 1000\times$ fainter at similar phases. If the X-ray or UV radiation powering the $H\alpha$ emission is similarly weak in these objects, the corresponding MIR emission would not be detectable, consistent with our non-detections in *NEOWISE* data (Figure 4).

In our VLA follow-up observation of SN 2022bbt at 932 days post-explosion, we did not detect a radio source, with a 5σ flux density limit of $F_\nu < 31 \mu\text{Jy}$ at a fre-

quency of 5.5 GHz. Adopting the formalism of Chomiuk et al. (2016) for $p = 3$, we infer the density of the environment assuming both ISM ($\rho_{\text{ISM}} \propto \text{constant}$) and wind-like ($\rho_{\text{CSM}} \propto r^{-2}$) environments. We assume we are in equipartition with shock microphysical parameters with $\epsilon_e = \epsilon_B = 0.1$. For SN 2022bbt, we constrain the mass loss rate for a wind-like environment to be $\dot{M} < 2 \times 10^{-6} M_\odot \text{ yr}^{-1}$ for a wind velocity of $v_w = 10 \text{ km s}^{-1}$. We constrain the density for an ISM environment to be $n < 200 \text{ cm}^{-3}$.

We can similarly use our limits on the intermediate-width $H\alpha$ luminosity $L_{H\alpha}^{\text{Inter}}$ to constrain the mass loss rate, following Equation 2 in Salamanca et al. (1998) which states

$$L_{H\alpha}^{\text{Inter}} = \frac{1}{4} \epsilon_{H\alpha} \frac{v_s^3}{v_w} \dot{M}, \quad (3)$$

where v_s is the shell ejecta velocity, v_w is the wind velocity, \dot{M} is the mass loss rate, and $\epsilon_{H\alpha}$ is an efficiency factor. Using $v_s = 10000 \text{ km s}^{-1}$ for the shell ejecta, $v_w = 10 \text{ km s}^{-1}$ for the wind, and a fiducial value of $\epsilon_{H\alpha} = 0.01$, we find a mass loss limit of $\dot{M} < 4.8 \times 10^{-5} M_\odot \text{ yr}^{-1}$ for SN 2020yex and $\dot{M} < 1.2 \times 10^{-6} M_\odot \text{ yr}^{-1}$ for SN 2022bbt. We note that the efficiency factor $\epsilon_{H\alpha}$ is a poorly constrained value that is estimated to be ≈ 0.1 at early times, but eventually drops to zero (Salamanca et al. 1998). We choose $\epsilon_{H\alpha} = 0.01$ since our measurements are at very late times. These limits are consistent with the radio measurements presented above.

4. DISCUSSION AND SUMMARY

Our sample of five SNe with MIR signatures of delayed CSM interaction nearly doubles the previously known population, and in particular, substantially increases the diversity of SN Ia sub-types known to exhibit late CSM interaction. We can roughly estimate the fraction of SNe Ia showing late-time MIR brightening by considering SN 2021jun, which was included in the flux-limited ZTF Bright Transient Survey (BTS; spectroscopically complete to 18.5 mag; Fremling et al. 2020; Perley et al. 2020). We restrict the BTS sample to SNe classified between 2018 June to 2021 June that pass BTS sample cuts (Perley et al. 2020), to allow for at least 1.5 years of *NEOWISE* observations after the discovery of the SN. This results in a sample of 1466 SNe Ia, out of which we find one exhibiting late-time MIR brightening. We therefore set a lower limit of 0.05% on the fraction of SNe Ia which exhibit delayed CSM interaction within 1.5 yr of explo-

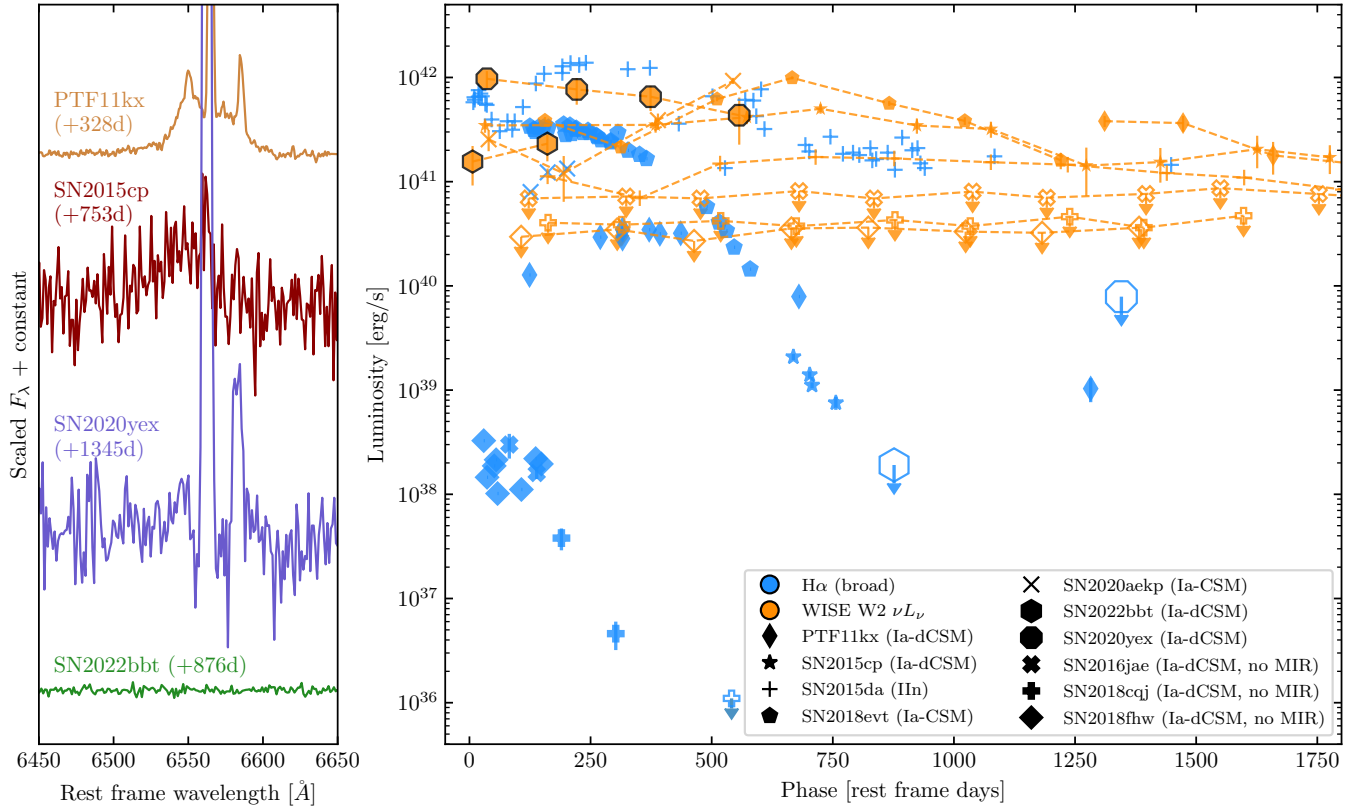


Figure 4. Optical spectroscopic and mid-infrared photometric signatures of CSM interaction. *Left:* Spectra of the known delayed CSM-interacting SNe PTF11kx (Graham et al. 2017) and SN 2015cp (Graham et al. 2019), compared to spectra we obtained for SN 2020yex and SN 2022bbt, zoomed into the region around H α . Both H α lines (> 1000 km s $^{-1}$) from CSM interaction, as well as unresolved host galaxy lines, are visible for PTF11kx and SN 2015cp. In contrast, only narrow lines from the host galaxy are visible for SN 2020yex, while no trace is detected in SN 2022bbt. *Right:* Comparison of the evolution of mid-infrared (*NEOWISE*; orange) and H α (blue) luminosity for SNe Ia displaying delayed CSM interaction (labeled Ia-dCSM in the legend). We also show the corresponding luminosity evolution for SN 2015da (SN IIn; Tartaglia et al. 2020), SN 2018evt (SN Ia-CSM; Wang et al. 2024), SN 2020aekp (SN Ia-CSM; Sharma et al. 2023) and three SNe Ia which show late-time nebular H α emission (SN 2016jae; Elias-Rosa et al. 2021, SN 2018cqj; Prieto et al. 2020, and SN 2018flw; Kollmeier et al. 2019; Valley et al. 2019). We show 5σ upper limits on the broad/intermediate H α line (see Appendix B) for two events in our sample in blue as the empty hexagon and square respectively.

sion.¹⁰ This is comparable with the rate of SNe Ia-CSM found by Silverman et al. (2013a), Dilday et al. (2012), and Sharma et al. (2023) via searches around peak-light, indicating a similar fraction of SNe Ia exhibiting delayed interaction with CSM shells at $\sim 10^{16} - 10^{17}$ cm. This is also consistent with the upper limits on rates of late-onset CSM interaction estimated from GALEX data by Dubay et al. (2022).

¹⁰ This is a lower limit due to our restrictive filtering criteria, which may have excluded interacting SNe Ia that are coincident with complex galaxy backgrounds, active galactic nuclei hosts, or where the brightening was missed in the *NEOWISE* observing gaps. Additionally, SN 2021jun is a member of the underluminous Iax sub-class, indicating a potentially larger rate among SNe Iax compared to the broader SNe Ia population.

The presence of pre-existing dust disfavors the classical double-degenerate progenitor model for SNe Ia, which are usually assumed to occur in clean environments (Maoz et al. 2014; Taubenberger 2017). Instead, the existence of (potentially multiple) detached CSM shells indicate recent intense mass loss episodes that ended shortly prior to the explosion, which could arise in either a single degenerate scenario (via recurrent novae; Hachisu et al. 1999; Sokoloski et al. 2006; Dilday et al. 2012; Moore & Bildsten 2012; Dimitriadis et al. 2014), or a core-degenerate model with variable mass-loss rates during common-envelope (CE) ejection (Livio & Riess 2003; Soker et al. 2013; Soker & Bear 2023). The dust mass lower limits inferred from photometry ($\sim 10^{-6} - 10^{-4} M_\odot$) suggest lower limits on total CSM masses of $\sim 10^{-4} - 10^{-2} M_\odot$ assuming a gas-to-dust mass ratio of

≈ 100 . On the high end, these lower limits on the masses may be similar to that estimated for PTF11kx (Dilday et al. 2012), which was argued by Soker et al. (2013) to be too massive to be explained by recent nova shells, though nova shells may be suitable for situations with lower CSM masses. Similarly, the delayed dynamical instability model by Han & Podsiadlowski (2006), which invokes dynamical mass transfer at the time of explosion, cannot explain the time-delay between the explosion and the onset of CSM interaction.

Since our sample of SNe do not show signatures of interaction around the time of spectroscopic classification at peak light, the closest CSM shells must be farther than the ejecta radius at that time. For a typical classification phase of ~ 20 d after explosion and an ejecta velocity of $10\,000\text{ km s}^{-1}$, this sets a lower limit on the minimum CSM radius of $\gtrsim 10^{15}$ cm. Since the interaction appears to have begun by $\sim 100\text{--}300$ d after explosion (Figure 3), we constrain the CSM to be located at $\sim 10^{15} - 2 \times 10^{16}$ cm. If the gas-to-dust mass ratio is significantly lower than the ≈ 100 assumed above, the total CSM mass may be explainable by recurrent novae. Given the minimum CSM radius of $\sim 10^{15}$ cm and a nova shell velocity of $\sim 1000\text{ km s}^{-1}$ (Aydi et al. 2020), the ejection of the last nova shell must have occurred $\sim 0.5 - 3$ yr prior to explosion.

In the core-degenerate case that may better explain larger CSM masses, slower CE ejection velocities of 10 km s^{-1} (Soker 2019) indicate that the CE was ejected $\sim 50 - 300$ yr prior to explosion, consistent with the constraint by Soker (2019) from SN 2015cp (Graham et al. 2019). Our derived rate for late CSM interaction, which we find to be similar to that of SNe Ia showing prompt CSM interaction (SNe Ia-CSM), support the claim in Soker (2022) that the time delay distribution between CE ejection and explosion may be more likely to be constant than the $\propto t^{-1}$ rate that is predicted for the delay time since star formation (Friedmann & Maoz 2018; Heringer et al. 2019). Soker (2019) predicts that $\approx 10\%$ of SNe Ia should experience ejecta-CSM interaction within 30 yr. Applying a flat time delay distribution to this prediction suggests that $\approx 0.5\%$ of SNe Ia show CSM interaction within 1.5 yr, similar to our lower limit of $\gtrsim 0.1\%$. In another single-degenerate model, Justham (2011) suggests that a rapidly-rotating super-Chandrasekhar WD can remain stable until after its donor’s H-rich envelope is exhausted and contracts or is ejected, leading to a delayed explosion with little-to-no observable interaction at early times, in line with our observations.

Over half of our sample is comprised of overluminous 91T-like and super-Chandra SNe Ia¹¹, despite their intrinsic rarity—with 91T-like events and super-Chandra events representing only $\approx 12\%$ and 0.8% of all SNe Ia respectively (Dimitriadis et al. 2024). Since the overluminous and long-lived nature of their optical light curves suggests that these SNe have progenitors that are more massive than those of typical SNe Ia, their connection to delayed CSM interaction presented here points at a potential double degenerate scenario where the merger and subsequent explosion happens very shortly after the end of the CE phase (Scalzo et al. 2010; Raskin et al. 2014; Siebert et al. 2024). The lower fraction of normal SNe Ia exhibiting delayed CSM interaction then may point to a longer delay from the end of the common envelope to the time of explosion, if they also arise from the double degenerate channel.

The connection between a SN Iax and a potential helium star companion (in SN 2012Z; McCully et al. 2022) suggests that the late interaction seen in the Type Iax SN 2021jun could be with circumstellar He, in a scenario similar to the helium-rich CSM surrounding SN 2020eyj (Kool et al. 2023). While Kool et al. (2023) favored a single-degenerate He star channel for SN 2020eyj, Soker & Bear (2023) suggested that it could also be explained by a core-degenerate scenario where the last common envelope was produced by expansion and subsequent ejection of the He-rich envelope. Future MIR observations with *JWST* that are sensitive to the total dust mass via MIR continuum measurements may be able to distinguish between these scenarios based on the differing predictions for the total CSM mass in these two cases (Moriya et al. 2019). In addition, our existing observations cannot rule out MIR emission purely from massive dust echoes with particular geometries; future *JWST* observations can also explore this possibility. While our search was aided by the (short) overlap between systematic optical SN searches and the *NEOWISE* survey, we demonstrate that the luminous and long-lived IR signatures of CSM interaction provide a powerful probe of the environments of SNe Ia—suggesting that ground-based IR surveys like *WINTER* (Lourie et al. 2020; Frostig et al. 2024) and *PRIME* (Yama et al. 2023), as well as space-based surveys like *NEO-Surveyor* (Mainzer et al. 2023) and the *Roman* space telescope (Rose et al. 2021) are poised to systematically reveal this population.

¹¹ PTF11kx and SN 2015cp were also initially classified as SNe Ia-91T at early phases, as are most known SNe Ia-CSM at very early phases (Phillips et al. 2024).

We would like to acknowledge useful discussions with Melissa Graham, Wenbin Lu, Ken Shen, Joel Johansson and Kiyoshi Masui. We thank Kristin Chiboucas for her excellent support with Gemini observations. G. M. acknowledges the support of the National Science Foundation and the LIGO Laboratory. K. D. was supported by NASA through the NASA Hubble Fellowship grant #HST-HF2-51477.001 awarded by the Space Telescope Science Institute, which is operated by the Association of Universities for Research in Astronomy, Inc., for NASA, under contract NAS5-26555. K. D. acknowledges support from a MIT Kavli Institute Fellowship.

This work is based on observations obtained at the international Gemini Observatory, a program of NSF NOIRLab, which is managed by the Association of Universities for Research in Astronomy (AURA) under a cooperative agreement with the U.S. National Science Foundation on behalf of the Gemini Observatory partnership: the U.S. National Science Foundation (United States), National Research Council (Canada), Agencia Nacional de Investigación y Desarrollo (Chile), Ministerio de Ciencia, Tecnología e Innovación (Argentina), Ministério da Ciência, Tecnologia, Inovações e Comunicações

(Brazil), and Korea Astronomy and Space Science Institute (Republic of Korea). This work was enabled by observations made from the Gemini North telescope, located within the Maunakea Science Reserve and adjacent to the summit of Maunakea. We are grateful for the privilege of observing the Universe from a place that is unique in both its astronomical quality and its cultural significance.

This paper includes data gathered with the 6.5 meter Magellan Telescopes located at Las Campanas Observatory, Chile.

The National Radio Astronomy Observatory is a facility of the National Science Foundation operated under cooperative agreement by Associated Universities, Inc.

Facilities: NEOWISE, Gemini:Gillett (GMOS), VLA, Magellan:Baade (FIRE, FourStar), WINTER, PO:1.2m, ZTF, ATLAS, Gaia, Spitzer

Software: `astropy` (Robitaille et al. 2013), `matplotlib` (Hunter 2007), `numpy` (Harris et al. 2020), `pandas` (pandas development team 2020; McKinney 2010), `pypeit` (Prochaska et al. 2020), `scipy` (Virtanen et al. 2020),

REFERENCES

- Ablimit, I. 2021, *PASP*, 133, 074201
- Ashall, C., Mazzali, P., Sasdelli, M., & Prentice, S. J. 2016, *MNRAS*, 460, 3529
- Avelino, A., Friedman, A. S., Mandel, K. S., et al. 2019, *ApJ*, 887, 106
- Aydi, E., Chomiuk, L., Izzo, L., et al. 2020, *ApJ*, 905, 62
- Bellm, E. C., Kulkarni, S. R., Graham, M. J., et al. 2018, *Publications of the Astronomical Society of the Pacific*, 131, 018002. <http://dx.doi.org/10.1088/1538-3873/aaecbe>
- Blondin, S., Matheson, T., Kirshner, R. P., et al. 2012, *AJ*, 143, 126
- Bochenek, C. D., Dwarkadas, V. V., Silverman, J. M., et al. 2018, *MNRAS*, 473, 336
- Branch, D., & Tammann, G. A. 1992, *ARA&A*, 30, 359
- Bulla, M., Liu, Z. W., Röpke, F. K., et al. 2020, *A&A*, 635, A179
- Chambers, K. C., Magnier, E. A., Metcalfe, N., et al. 2016, *arXiv e-prints*, arXiv:1612.05560
- Childress, M. J., Filippenko, A. V., Ganeshalingam, M., & Schmidt, B. P. 2014, *MNRAS*, 437, 338
- Chomiuk, L., Soderberg, A. M., Chevalier, R. A., et al. 2016, *The Astrophysical Journal*, 821, 119. <https://dx.doi.org/10.3847/0004-637X/821/2/119>
- Condon, J. J., Cotton, W. D., Greisen, E. W., et al. 1998, *AJ*, 115, 1693
- Coulter, D. A., Siebert, M. R., Pan, Y. C., et al. 2017, *The Astronomer’s Telegram*, 10601, 1
- De, K., Hankins, M. J., Kasliwal, M. M., et al. 2020, *Publications of the Astronomical Society of the Pacific*, 132, 025001. <http://dx.doi.org/10.1088/1538-3873/ab6069>
- De, K., Kasliwal, M. M., Tzanidakis, A., et al. 2020, *ApJ*, 905, 58
- Deckers, M., Maguire, K., Magee, M. R., et al. 2022, *MNRAS*, 512, 1317
- Dhawan, S., Jha, S. W., & Leibundgut, B. 2018, *A&A*, 609, A72
- Dilday, B., Howell, D. A., Cenko, S. B., et al. 2012, *Science*, 337, 942
- Dimitriadis, G., Chiotellis, A., & Vink, J. 2014, *MNRAS*, 443, 1370
- Dimitriadis, G., Burgaz, U., Deckers, M., et al. 2024, *arXiv e-prints*, arXiv:2409.04200
- Draine, B. T., & Li, A. 2001, *ApJ*, 551, 807
- . 2007, *ApJ*, 657, 810
- Dubay, L. O., Tucker, M. A., Do, A., Shappee, B. J., & Anand, G. S. 2022, *ApJ*, 926, 98
- Dwarkadas, V. V. 2023, *MNRAS*, 520, 1362
- . 2024, *MNRAS*, 533, 27
- Dye, S., Lawrence, A., Read, M. A., et al. 2018, *MNRAS*, 473, 5113

- Elias-Rosa, N., Chen, P., Benetti, S., et al. 2021, *A&A*, 652, A115
- Foley, R. J., Jha, S. W., Pan, Y.-C., et al. 2016, *MNRAS*, 461, 433
- Fox, O. D., Chevalier, R. A., Dwek, E., et al. 2010, *ApJ*, 725, 1768
- Fox, O. D., & Filippenko, A. V. 2013, *ApJL*, 772, L6
- Fox, O. D., Chevalier, R. A., Skrutskie, M. F., et al. 2011, *ApJ*, 741, 7
- Fox, O. D., Silverman, J. M., Filippenko, A. V., et al. 2015, *MNRAS*, 447, 772
- Fox, O. D., Johansson, J., Kasliwal, M., et al. 2016, *ApJL*, 816, L13
- Fremming, C., Miller, A. A., Sharma, Y., et al. 2020, *ApJ*, 895, 32
- Friedmann, M., & Maoz, D. 2018, *MNRAS*, 479, 3563
- Frostig, D., Burdge, K. B., De, K., et al. 2024, in *Ground-based and Airborne Instrumentation for Astronomy X*, Vol. 13096, SPIE, 1048–1068
- Goldwasser, S., Yaron, O., Sass, A., et al. 2022, *Transient Name Server AstroNote*, 191, 1
- Graham, M. L., Harris, C. E., Fox, O. D., et al. 2017, *ApJ*, 843, 102
- Graham, M. L., Harris, C. E., Nugent, P. E., et al. 2019, *ApJ*, 871, 62
- Gromadzki, M., Ihanec, N., Wevers, T., et al. 2020, *Transient Name Server AstroNote*, 211, 1
- Hachisu, I., Kato, M., & Nomoto, K. 1999, *ApJ*, 522, 487
- Hakobyan, A. A., Barkhudaryan, L. V., Karapetyan, A. G., et al. 2020, *MNRAS*, 499, 1424
- Han, Z., & Podsiadlowski, P. 2004, *MNRAS*, 350, 1301
- . 2006, *MNRAS*, 368, 1095
- Harris, C. E., Nugent, P. E., Horesh, A., et al. 2018, *ApJ*, 868, 21
- Harris, C. R., Millman, K. J., van der Walt, S. J., et al. 2020, *Nature*, 585, 357.
- <https://doi.org/10.1038/s41586-020-2649-2>
- Heringer, E., Pritchett, C., & van Kerkwijk, M. H. 2019, *ApJ*, 882, 52
- Hildebrand, R. H., Whitcomb, S. E., Winston, R., et al. 1977, *ApJ*, 216, 698
- Hiroi, K., Ueda, Y., Hayashida, M., et al. 2013, *ApJS*, 207, 36
- Hodgkin, S. T., Breedt, E., Delgado, A., et al. 2020, *Transient Name Server Discovery Report*, 2020-3256, 1
- Hodgkin, S. T., Harrison, D. L., Breedt, E., et al. 2021, *A&A*, 652, A76
- Hook, I. M., Jørgensen, I., Allington-Smith, J. R., et al. 2004, *PASP*, 116, 425
- Howell, D. A., Sullivan, M., Nugent, P. E., et al. 2006, *Nature*, 443, 308
- Hunter, J. D. 2007, *Matplotlib: A 2D graphics environment*, IEEE COMPUTER SOC, doi:10.1109/MCSE.2007.55
- Jarrett, T. H., Cohen, M., Masci, F., et al. 2011, *ApJ*, 735, 112
- Jencson, J. E., Kasliwal, M. M., Adams, S. M., et al. 2019, *ApJ*, 886, 40
- Jiang, N., Wang, T., Dou, L., et al. 2021, *ApJS*, 252, 32
- Johansson, J., Chu, M., Dahiwal, A., & Fremming, C. 2022, *Transient Name Server Classification Report*, 2022-1640, 1
- Justham, S. 2011, *ApJL*, 730, L34
- Karnesis, N., Babak, S., Pironi, M., Cornish, N., & Littenberg, T. 2021, *PhRvD*, 104, 043019
- Kasen, D., & Woosley, S. E. 2007, *ApJ*, 656, 661
- Kashi, A., & Soker, N. 2011, *MNRAS*, 417, 1466
- Kelsey, L. 2024, *MNRAS*, 527, 8015
- Kobayashi, C., & Nomoto, K. 2009, *ApJ*, 707, 1466
- Kochanek, C. S., Shappee, B. J., Stanek, K. Z., et al. 2017, *PASP*, 129, 104502
- Kollmeier, J. A., Chen, P., Dong, S., et al. 2019, *MNRAS*, 486, 3041
- Kool, E. C., Johansson, J., Sollerman, J., et al. 2023, *Nature*, 617, 477
- Korol, V., Buscicchio, R., Pakmor, R., et al. 2024, *arXiv e-prints*, arXiv:2407.03935
- Krimm, H. A., Holland, S. T., Corbet, R. H. D., et al. 2013, *ApJS*, 209, 14
- Lach, F., Röpke, F. K., Seitenzahl, I. R., et al. 2020, *A&A*, 644, A118
- Lang, D. 2014, *AJ*, 147, 108
- Leloudas, G., Hsiao, E. Y., Johansson, J., et al. 2015, *A&A*, 574, A61
- Liu, Z.-W., Röpke, F. K., & Han, Z. 2023, *Research in Astronomy and Astrophysics*, 23, 082001
- Livio, M., & Riess, A. G. 2003, *ApJL*, 594, L93
- Lourie, N. P., Baker, J. W., Burruss, R. S., et al. 2020, in *Society of Photo-Optical Instrumentation Engineers (SPIE) Conference Series*, Vol. 11447, Society of Photo-Optical Instrumentation Engineers (SPIE) Conference Series, 114479K
- Mainzer, A., Bauer, J., Cutri, R. M., et al. 2014, *ApJ*, 792, 30
- Mainzer, A. K., Masiero, J. R., Abell, P. A., et al. 2023, *PSJ*, 4, 224
- Maoz, D., Mannucci, F., & Nelemans, G. 2014, *ARA&A*, 52, 107
- Margutti, R., Parrent, J., Kamble, A., et al. 2014, *ApJ*, 790, 52

- McCully, C., Jha, S. W., Scalzo, R. A., et al. 2022, *ApJ*, 925, 138
- McKinney, W. 2010, Data structures for statistical computing in python, Proceedings of the 9th Python in Science Conference
- Meisner, A. M., Lang, D., & Schlegel, D. J. 2018, *AJ*, 156, 69
- Moore, K., & Bildsten, L. 2012, *ApJ*, 761, 182
- Moriya, T. J., Liu, D., Wang, B., & Liu, Z.-W. 2019, *MNRAS*, 488, 3949
- Moriya, T. J., Mazzali, P. A., Ashall, C., & Pian, E. 2023, *MNRAS*, 522, 6035
- Mulligan, B. W., & Wheeler, J. C. 2017, *MNRAS*, 467, 778
- Munoz-Arancibia, A., Forster, F., Bauer, F. E., et al. 2021, Transient Name Server Discovery Report, 2021-1208, 1
- Myers, C., De, K., Yan, L., et al. 2024, arXiv e-prints, arXiv:2405.14663
- Nagao, T., Maeda, K., & Yamanaka, M. 2017, *ApJ*, 835, 143
- Noebauer, U. M., Taubenberger, S., Blinnikov, S., Sorokina, E., & Hillebrandt, W. 2016, *MNRAS*, 463, 2972
- Nozawa, T., Maeda, K., Kozasa, T., et al. 2011, *ApJ*, 736, 45
- Onori, F., Cannizzaro, G., Knezevic, N., & Yaron, O. 2017, Transient Name Server Classification Report, 2017-1251, 1
- Pakmor, R., Kromer, M., Taubenberger, S., & Springel, V. 2013, *ApJL*, 770, L8
- pandas development team, T. 2020, pandas-dev/pandas: Pandas, vlatest, Zenodo, doi:10.5281/zenodo.3509134. <https://doi.org/10.5281/zenodo.3509134>
- Perley, D. A., Fremling, C., Sollerman, J., et al. 2020, *ApJ*, 904, 35
- Persson, S. E., Murphy, D. C., Smee, S., et al. 2013, *PASP*, 125, 654
- Phillips, M. M. 1993, *ApJL*, 413, L105
- Phillips, M. M., Ashall, C., Brown, P. J., et al. 2024, *ApJS*, 273, 16
- Planck Collaboration, Aghanim, N., Akrami, Y., et al. 2020, *A&A*, 641, A6
- Polin, A., Nugent, P., & Kasen, D. 2019, *ApJ*, 873, 84
- Postnov, K. A., & Yungelson, L. R. 2014, *Living Reviews in Relativity*, 17, 3
- Prieto, J. L., & Stanek, K. Z. 2017, Transient Name Server Discovery Report, 2017-802, 1
- Prieto, J. L., Chen, P., Dong, S., et al. 2020, *ApJ*, 889, 100
- Prochaska, J., Hennawi, J., Westfall, K., et al. 2020, *The Journal of Open Source Software*, 5, 2308
- Raskin, C., Kasen, D., Moll, R., Schwab, J., & Woosley, S. 2014, *ApJ*, 788, 75
- Rebassa-Mansergas, A., Toonen, S., Korol, V., & Torres, S. 2019, *MNRAS*, 482, 3656
- Robitaille, T. P., Tollerud, E. J., Greenfield, P., et al. 2013, *Astropy: A community Python package for astronomy*, EDP Sciences, doi:10.1051/0004-6361/201322068. <http://dx.doi.org/10.1051/0004-6361/201322068>
- Rose, B. M., Baltay, C., Hounsell, R., et al. 2021, arXiv e-prints, arXiv:2111.03081
- Ruiter, A. J. 2020, in *White Dwarfs as Probes of Fundamental Physics: Tracers of Planetary, Stellar and Galactic Evolution*, ed. M. A. Barstow, S. J. Kleinman, J. L. Provencal, & L. Ferrario, Vol. 357, 1–15
- Salamanca, I., Cid-Fernandes, R., Tenorio-Tagle, G., et al. 1998, *MNRAS*, 300, L17
- Scalzo, R. A., Aldering, G., Antilogus, P., et al. 2010, *ApJ*, 713, 1073
- Schulze, S., Johansson, J., Skan, M., et al. 2021, Transient Name Server Classification Report, 2021-1619, 1
- Sharma, Y., Sollerman, J., Fremling, C., et al. 2023, *ApJ*, 948, 52
- Siebert, M. R., Kwok, L. A., Johansson, J., et al. 2024, *ApJ*, 960, 88
- Silverman, J. M., Nugent, P. E., Gal-Yam, A., et al. 2013a, *ApJS*, 207, 3
- . 2013b, *ApJ*, 772, 125
- Simcoe, R. A., Burgasser, A. J., Schechter, P. L., et al. 2013, *PASP*, 125, 270
- Skan, M., Cehula, J., Schoelch, M., et al. 2021, Transient Name Server AstroNote, 159, 1
- Smith, N. 2017, in *Handbook of Supernovae*, ed. A. W. Alsabti & P. Murdin, 403
- Soker, N. 2019, *MNRAS*, 490, 2430
- . 2022, *Research in Astronomy and Astrophysics*, 22, 035025
- Soker, N., & Bear, E. 2023, *MNRAS*, 521, 4561
- Soker, N., Kashi, A., García-Berro, E., Torres, S., & Camacho, J. 2013, *MNRAS*, 431, 1541
- Sokoloski, J. L., Luna, G. J. M., Mukai, K., & Kenyon, S. J. 2006, *Nature*, 442, 276
- Stein, R. D., Karambelkar, V., Kishore, S., et al. 2024, *winter-telescope/mirar: v0.17.0, vv0.17.0*, Zenodo, doi:10.5281/zenodo.13352565. <https://doi.org/10.5281/zenodo.13352565>
- Szalai, T., & Vinkó, J. 2013, *A&A*, 549, A79
- Szalai, T., Zsíros, S., Fox, O. D., Pejcha, O., & Müller, T. 2019, *ApJS*, 241, 38
- Szalai, T., Fox, O. D., Arendt, R. G., et al. 2021, *ApJ*, 919, 17
- Tartaglia, L., Pastorello, A., Sollerman, J., et al. 2020, *A&A*, 635, A39
- Taubenberger, S. 2017, in *Handbook of Supernovae*, ed. A. W. Alsabti & P. Murdin, 317

- Terwel, J. H., Maguire, K., Dimitriadis, G., et al. 2024, arXiv e-prints, arXiv:2402.16962
- Thévenot, M., Gantier, J. M., Kabatnik, M., Schümann, J., & Gramaize, L. 2021a, Research Notes of the American Astronomical Society, 5, 58
- Thévenot, M., Kabatnik, M., & Gantier, J. M. 2021b, Transient Name Server AstroNote, 212, 1
- Tonry, J., Stalder, B., Denneau, L., et al. 2017, Transient Name Server Discovery Report, 2017-1236, 1
- Tonry, J., Denneau, L., Heinze, A., et al. 2020, Transient Name Server Discovery Report, 2020-1827, 1
- Tonry, J., Denneau, L., Weiland, H., et al. 2022, Transient Name Server Discovery Report, 2022-255, 1
- Tonry, J. L., Denneau, L., Heinze, A. N., et al. 2018, PASP, 130, 064505
- Toonen, S., Nelemans, G., & Portegies Zwart, S. 2012, A&A, 546, A70
- Tucker, M. A. 2022, Transient Name Server Classification Report, 2022-344, 1
- Tutukov, A. V., Yungelson, L. R., & Iben, Icko, J. 1992, ApJ, 386, 197
- Vallely, P. J., Fausnaugh, M., Jha, S. W., et al. 2019, MNRAS, 487, 2372
- Virtanen, P., Gommers, R., Oliphant, T. E., et al. 2020, Nature Methods, 17, 261
- Wang, B., & Han, Z. 2012, NewAR, 56, 122
- Wang, L., Hu, M., Wang, L., et al. 2024, Nature Astronomy, 8, 504
- Werner, M. W., Roellig, T. L., Low, F. J., et al. 2004, ApJS, 154, 1
- Wright, E. L., Eisenhardt, P. R. M., Mainzer, A. K., et al. 2010, AJ, 140, 1868
- Yama, H., Suzuki, D., Miyazaki, S., et al. 2023, Journal of Astronomical Instrumentation, 12, 2350004
- Zackay, B., Ofek, E. O., & Gal-Yam, A. 2016, ApJ, 830, 27

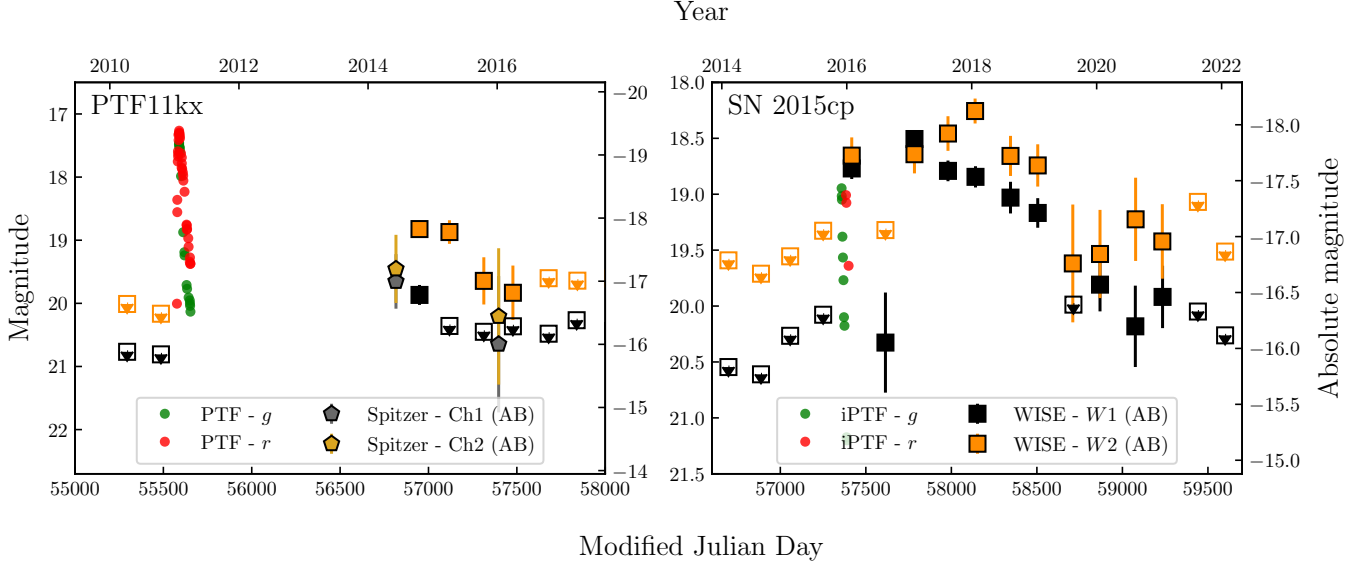


Figure A1. Optical and mid-infrared light curves of PTF11kx and SN 2015cp. We present *NEOWISE* photometry extracted using our difference imaging pipeline. We also show optical data from the Palomar Transient Factory (PTF; Dilday et al. 2012) and MIR data from *Spitzer* for PTF11kx (Graham et al. 2017). The *NEOWISE* and *Spitzer* photometry are marginally offset, which can be attributed to differences in filters between each instrument (Jarrett et al. 2011). For SN 2015cp, we show optical data from the intermediate PTF (iPTF; Graham et al. 2019).

Table A1. Number of candidates for MIR-identified delayed CSM interaction removed at each stage of the filtering process.

Filtering criterion	Filtered candidates	Remaining candidates
Initial sample from the Transient Name Server		8572
No detections prior to the optical SN onset and no obvious subtraction artifacts	8434	138
At least two <i>NEOWISE</i> epochs (≈ 1 yr) and rising MIR emission	120	18
Not a known SN Ia-CSM or SN Ia with delayed CSM interaction	12	6
<i>NEOWISE</i> imaging not from temporally coincident nuclear activity	1	5

APPENDIX

A. ARCHIVAL OBJECTS AND NEW SAMPLE DETAILS

We show optical and MIR light curves of PTF11kx and SN 2015cp in Figure A1, and details of our sample filtering in Table A1. We also show *NEOWISE* W2 reference, stack, and subtraction images in Figure A2.

SN 2017fra—SN 2017fra/ASASSN-17jq was discovered by ASAS-SN and was also observed by ATLAS and Gaia (Prieto & Stanek 2017). Coulter et al. (2017) spectroscopically classified it as a SN Ia-91T at -8 d. It resides in a late-type galaxy that may be interacting with a companion and is at a redshift of $z = 0.03$, resulting in a projected offset of 1.3 kpc. Jiang et al. (2021) first identified a connection between a MIR excess in its host and SN 2017fra, reporting single-epoch dust fits. This MIR emission was also identified by Thévenot et al. (2021a), who also noticed that SN 2017fra has a sibling in SN 2016cda (Kelsey 2024).¹² In addition to the MIR data presented in Jiang et al. (2021), we show five additional *NEOWISE* detection epochs in Figures 1 and 2. The MIR emission rises and fades smoothly over ≈ 5 yrs,

¹² SN 2016cda was the original candidate which appeared in our search, but the temporal coincidence of the MIR emission with SN 2017fra makes it the more likely association.

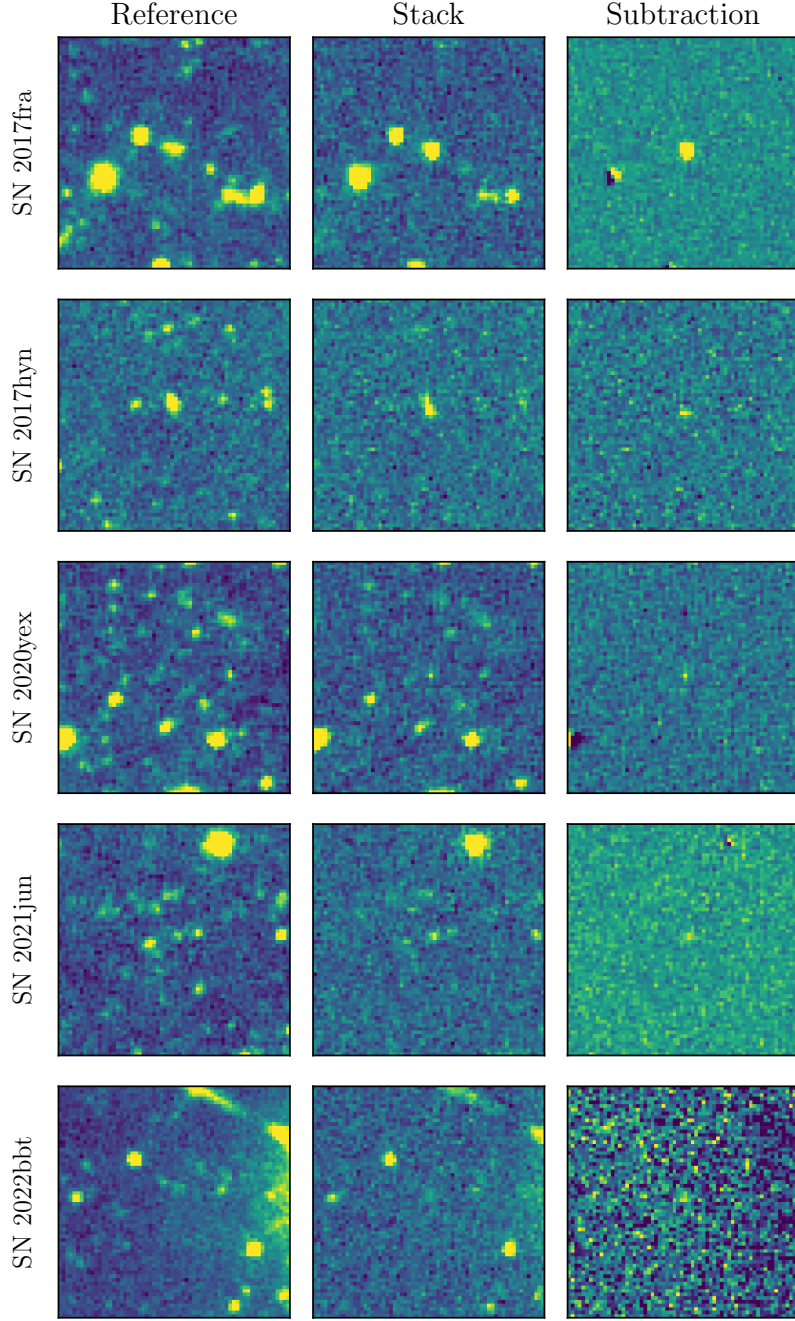


Figure A2. *NEOWISE* W2 reference, stacked science, and subtraction cutouts of our sources at their brightest epoch. Each cutout has a width and height of $3'$ centered at the location of the transient, aligned north up and east left.

peaking at $M_{\text{Vega},W2} \approx -22.3$ within ≈ 1.5 yrs after explosion; SN 2017fra is the most luminous MIR SN Ia (Figures 1 and 2).

SN 2017hyn—SN 2017hyn was discovered by ATLAS and also observed by Gaia (Tonry et al. 2017). It was spectroscopically classified as a Ia-91T by Onori et al. (2017) and is hosted in an edge-on disk galaxy at $z = 0.053$, for a projected offset of 8.3 kpc. Thévenot et al. (2021a) first noted a *NEOWISE* detection coincident with the optical peak, which is observed shortly after peak light. The subsequent long-lived MIR emission is similar to that of SN 2017fra, exhibiting a sharp peak at 1.5 years after explosion.

SN 2020yex—SN 2020yex was discovered by Gaia (Hodgkin et al. 2020) and classified as a Ia-91T by Gromadzki et al. (2020). It resides in a blue spheroidal galaxy with no distinct structure at $z = 0.087$ and is at a projected offset of 2.7 kpc. The MIR emission was first identified by Thévenot et al. (2021b), who noted that the *W1* luminosity was consistent with that of SNe Ia-CSM. Unlike the other MIR light curves in our sample, the *NEOWISE* *W2* light curve is consistent with a long-lived monotonic decline but the *W1* light curve exhibits a peak at ≈ 1.5 yr after the explosion.

SN 2021jun—SN 2021jun was discovered by ZTF (Munoz-Arancibia et al. 2021) as part of its Bright Transient Survey, also observed by ATLAS and Pan-STARRS, and classified by Skan et al. (2021); Schulze et al. (2021) as a SN Iax. Its host is blue and spheroidal at $z = 0.04$, with the SN at a projected offset of < 1 kpc. *NEOWISE* observations reveal brightening MIR emission six months after the SN, coincident with a faint rebrightening in the ZTF photometry. The MIR light curve color changes dramatically ≈ 1 yr later, becoming significantly more blue, after which it reddens again.

SN 2022bbt—SN 2022bbt was discovered by ATLAS (Tonry et al. 2022) and also observed by Pan-STARRS, Gaia, and ZTF in its Bright Transient Survey. It is offset ($7.3''$, 7.9 kpc projected distance at $z = 0.049$) from a face-on spiral host. Tucker (2022) classify it as a SN Ia, while Johansson et al. (2022) classify it as a Ia-pec. Using the spectrum from Tucker (2022) and the supernova fitting code NGSF (Goldwasser et al. 2022), we find evidence for low velocity C II lines, which together with the luminous (peaking at $M \approx -20$ AB mag in *r*-band) light curve, is consistent with SN 2022bbt being a super-Chandrasekhar (09dc-like) SN Ia (Howell et al. 2006). Since this is most recent event in our sample, only one *NEOWISE* detection is available; however, the luminosity is consistent with the rest of the population (Figure 1).

B. ADDITIONAL FOLLOW-UP OBSERVATIONS

We acquired Gemini GMOS-N (Hook et al. 2004) spectra on UT 2024-08-07 (SN 2022bbt) and Gemini GMOS-S spectra on UT 2024-10-26 (SN 2020yex) using the B480 gratings and 2×2 binning on the Hamamatsu detectors, resulting in 1.3 \AA spectral resolution, sufficient for distinguishing narrow host lines from the broad or intermediate lines indicative of SN ejecta. The sources were acquired using blind-offsets from nearby stars and each spectrum was integrated for 80 min. The spectra were reduced using standard routines in *PyPeIt* (Prochaska et al. 2020), including flat-fielding and wavelength calibration using arcs. Flux calibration was performed using a standard star observation followed by one-dimensional spectral extraction at the expected position of each SN. No broad or intermediate emission lines were identified in either spectrum (see Section 3.3). For each source, we derived an upper limit on the intermediate emission line flux by rebinning the spectrum to the expected $\sim 20 \text{ \AA}$ width ($\text{FWHM} \approx 1000 \text{ km s}^{-1}$) of the intermediate emission line (Graham et al. 2017), then taking the standard deviation of a $\sim 300 \text{ \AA}$ featureless section of the spectrum near the expected $\text{H}\alpha$ line.

We additionally attempted infrared spectroscopy of SN 2020yex with the FIRE (Simcoe et al. 2013) spectrograph on the Magellan/Baade telescope on UT 2024-07-04 in the low-resolution prism mode. The source was acquired using a blind-offset from a nearby star. No trace was detected at the source position with a total integration time of ≈ 20 min. We acquired NIR imaging in *J* and *Ks* bands of SN 2017fra on UT 2024-07-09 using the Fourstar (Persson et al. 2013) camera on the Magellan/Baade telescope. The dithered images (amounting to a total exposure time of ≈ 1200 s and ≈ 900 s in *J* and *Ks* bands, respectively) were stacked, astrometrically and photometrically calibrated using a custom pipeline (De et al. 2020). No source was detected at the SN position in the stacked images down to a 5σ limiting magnitude of > 20.5 Vega mag and > 19.0 Vega mag in *J* and *Ks* bands, respectively. We caution that these limits are derived from aperture photometry (together with visual inspection) at the SN position since there are no archival images of the quiescent host galaxy at this depth.

We observed SN 2021jun in the NIR *J*-band with the *WINTER* camera (Lourie et al. 2020; Frostig et al. 2024) mounted on the Palomar 1-m telescope on UT 2024-05-12, with a total exposure time of 3600 s. The images were processed using the *WINTER* data reduction pipeline *mirar* (Stein et al. 2024) and image subtraction was performed relative to *J*-band images from the UKIRT Hemisphere Survey (Dye et al. 2018). No sources were detected in difference imaging at the location of SN 2021jun, with a 5σ limiting magnitude of $J \sim 20.1$ (AB).

We also searched for radio emission from SN 2022bbt using the VLA (Condon et al. 1998) on UT 2024-08-28 in C-band, with the array in B-configuration ($1''$ beamwidth, to distinguish between host galaxy nuclear emission). We used 3C286 as a flux calibrator, while using J1516+1932 as a phase calibrator. The data was calibrated with the VLA CASA Calibration Pipeline using CASA 6.5.4. and imaged manually with the *TCLEAN* task in CASA, using natural weighting. No radio source was detected, with a 5σ flux density limit of $F_\nu < 31 \mu\text{Jy}$.